Inorganic Chemistry

pubs.acs.org/IC

Article

High-Pressure Synthesis of Semiconducting $PbCu_3Mn_4O_{12}$ with Near-Room-Temperature Ferrimagnetic Order

Haoting Zhao, Dabiao Lu, Xiao Wang, Xubin Ye, Jie Zhang, Maocai Pi, Zhao Pan, Yi-Ying Chin, Chien-Te Chen, Zhiwei Hu, and Youwen Long*

Cite This: *Inorg. Chem.* 2024, 63, 5924−5930

Read Online

ACCESS | Metrics & More | Article Recommendations

ABSTRACT: A transition-metal oxide of $PbCu_3Mn_4O_{12}$ was prepared at 1523 K and 10 GPa. An A-site-ordered quadruple perovskite structure with the space group $Im\bar{3}$ is assigned for this compound. Based on bond-valence-sum calculations and X-ray absorption spectroscopy, the charge combination is determined to be $PbCu_3^{2+}Mn_4^{4+}O_{12}$. Due to $Cu^{2+}(\uparrow)-Mn^{4+}(\downarrow)$ antiferromagnetic coupling, a near-room-temperature ferrimagnetic phase transition is observed at approximately 287 K. $PbCu_3Mn_4O_{12}$ exhibits a semiconducting electric transport property with the energy band gap $E_g \approx 0.2$ eV. In addition, considerable low-field magnetoresistance effects are observed at lower temperatures. This study provides an intrinsic near-room-temperature ferrimagnetic semiconductor that exhibits potential applications in next-generation spintronic devices.

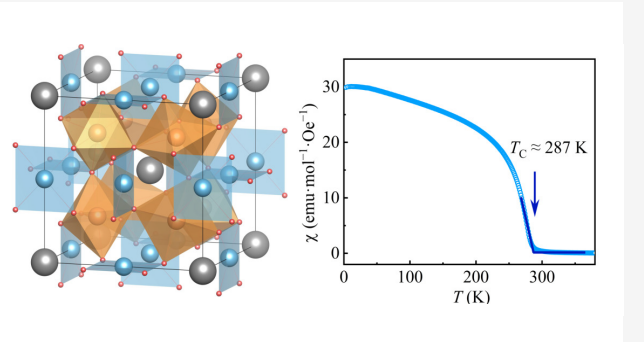

1. INTRODUCTION

A-site-ordered quadruple perovskite oxides with the formula $AA'_3B_4O_{12}$ have garnered widespread attention due to their peculiar crystal construction and intriguing physical and chemical properties.[1−10] In this specially ordered perovskite, the A site is typically occupied by rare-earth, alkaline-earth-metal, and/or alkali-metal ions, forming AO_{12} icosahedral units. In contrast, the A′ site is favorable for accommodating Jahn−Teller distortion ions such as Cu^{2+} and Mn^{3+}, forming square-planar coordinated $A'O_4$ units. Transition-metal ions often occupy the B site, forming corner-sharing BO_6 octahedra. Compared to simple perovskite oxides ABO_3, $AA'_3B_4O_{12}$ quadruple perovskites exhibit fascinating magnetic and electric transport properties because transition metals can be accommodated at both the A′ and B sites. For example, A′−B intersite charge transfer accompanied with negative thermal expansion is found to occur in $LaCu_3Fe_4O_{12}$,[7] magnetoelectric multiferroicity is observed in $LaMn_3Cr_4O_{12}$,[2] and large ferroelectric polarization and significant magnetoelectric coupling effects are both observed in $BiMn_3Cr_4O_{12}$.[1]

It is well-known that spin and charge degrees of freedom are compatible with each other in ferromagnetic or ferrimagnetic semiconductors, which can be used to develop advanced spintronic devices.[11−13] However, the number of ferromagnetic/ferrimagnetic semiconductors with Curie temperatures (T_C) that are close to or even higher than room temperature is limited at present. The above-mentioned $AA'_3B_4O_{12}$ quadruple perovskite oxides are promising candidates for exploring room-temperature ferromagnetic or ferrimagnetic semiconductors due to the diverse A′−B transition-metal ionic combinations. In fact, $CaCu_3Mn_4O_{12}$ is a well-known example that shows semiconducting conductivity and a T_C as high as 355 K.[14] There are numerous studies on $CaCu_3Mn_4O_{12}$ and its derivatives with A-site trivalent ionic substitution in the past decades.[15−20] In comparison, A-site substitution using divalent cations is relatively rare (only $Cd^{2+}Cu_3Mn_4O_{12}$ and $Mn^{2+}Cu_3Mn_4O_{12}$ so far).[21,22] The substitution of Cd^{2+} into $CdCu_3Mn_4O_{12}$ has an impact on the density of states close to the Fermi level, resulting in the emergence of metallic behavior. As for $MnCu_3Mn_4O_{12}$, the spin ordering of Mn^{2+} at the A site induces a broadening dome in the magnetic susceptibility around 200 K and reduces the magnitude of resistivity. These observations suggest that magnetic and electric transport properties can be manipulated through A-site equivalent substitution. Because Pb^{2+} has an electronic configuration ($6s^2$ lone-pair electrons) and an ionic radius different from those of Ca^{2+}, Cd^{2+}, and Mn^{2+} ions,[23,24] it is

Received: December 19, 2023
Revised: February 20, 2024
Accepted: March 8, 2024
Published: March 21, 2024

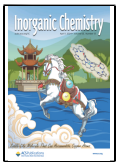

interesting to study the substitution effects of Pb^{2+} in the $ACu_3Mn_4O_{12}$ family. In this study, we report the synthesis of polycrystalline $PbCu_3Mn_4O_{12}$, a quadruple perovskite, for the first time using high-pressure and high-temperature conditions. The crystal structure, charge combination, and magnetic and electrical properties of the material are thoroughly investigated.

2. EXPERIMENTAL SECTION

For the synthesis of $PbCu_3Mn_4O_{12}$, high-purity PbO (Alfa, 99.99%), CuO (Alfa, 99.995%), and MnO_2 (Alfa, 99.9%) powders were selected. The powders were meticulously mixed and ground in a molar ratio of 1:3:4 in an argon-filled glovebox, ensuring an inert atmosphere throughout the process. Subsequently, approximately 150 mg (equivalent to 0.185 mmol) of the thoroughly mixed powders was carefully sealed inside a platinum capsule measuring 3 mm in diameter and 4 mm in height. Note that these two procedures should be performed in a glovebox due to the toxicity of PbO. Then, the platinum capsule containing the mixed powders was subjected to high-pressure and high-temperature treatment using a cubic anvil-type high-pressure device. The treatment involved applying a pressure of 10 GPa and heating the capsule to 1523 K for a duration of 60 min. Following the reaction, the sample was rapidly cooled to room temperature, and the high pressure was gradually released over a period of 10 h until reaching ambient pressure. The crystal structure of $PbCu_3Mn_4O_{12}$ was determined using powder X-ray diffraction (XRD) analysis. A Huber X-ray diffractometer, operating at 40 kV and 30 mA, with Cu $K\alpha_1$ radiation, was employed. The XRD measurements were conducted in the 2θ range from 10 to 100°, with a step of 0.005°. The *GSAS* program was used to carry out the Rietveld refinement.[25] X-ray absorption spectroscopy (XAS) at the Cu $L_{2,3}$- and Mn $L_{2,3}$-edges was collected at the BL11A beamline of the NSRRC in Taiwan. A magnetic property measurement system (MPMS-VSM, Quantum Design) was used to measure the magnetic susceptibility and magnetization. An applied field of 1000 Oe at 2−380 K was used to collect the magnetic susceptibility data for both field-cooled (FC) and zero-field-cooled (ZFC) modes. Field-dependent isothermal magnetization was measured at temperatures of 2, 150, and 350 K, with applied fields varying from −5 to +5 T. Specific heat, resistivity, and magnetoresistance (MR) measurements were performed utilizing a physical property measurement system (PPMS, Quantum Design). Electric transport measurements were carried out using the standard four-probe method.

3. RESULTS AND DISCUSSION

Figure 1a displays the powder XRD pattern and the results of the Rietveld refinement for $PbCu_3Mn_4O_{12}$ at room temperature. According to the refinements, $PbCu_3Mn_4O_{12}$ crystallized in an A-site-ordered quadruple perovskite structure with the space group $Im\bar{3}$, which is isostructural with that of $CaCu_3Mn_4O_{12}$.[14] In this symmetry, Pb and Cu atoms are arranged in a 1:3 order at the specific Wyckoff sites 2a (0, 0, 0) and 6b (0, 0.5, 0.5), respectively. The Mn atoms at the B site occupy specific Wyckoff site 8c (0.25, 0.25, 0.25), exhibiting MnO_6 octahedral coordination. The O atoms are located at 24g (0, y, z). It is worth noting that the A′-site Cu atoms exhibit square-planar CuO_4 coordination due to the Jahn−Teller effect,[27] which is in contrast to the 12-coordinated A-site Pb atoms. Figure 1b shows the schematic crystal structure of $PbCu_3Mn_4O_{12}$, where corner-sharing MnO_6 and square-planar CuO_4 units connect to each other. Table 1 presents the refined structure parameters for $PbCu_3Mn_4O_{12}$, such as the lattice constant, atomic positions, chosen bond lengths, and bond angles. $PbCu_3Mn_4O_{12}$ has a larger lattice constant a [7.28930(1) Å] compared to $CaCu_3Mn_4O_{12}$ (7.241 Å) due to the larger ionic size of Pb.[28,29] In addition, the O−Cu−O bond angles in $PbCu_3Mn_4O_{12}$ (93.6°/86.4°) are smaller than

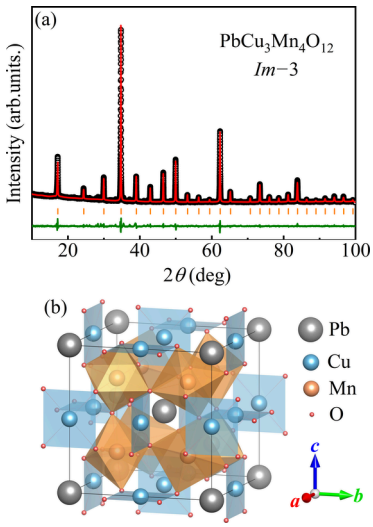

Figure 1. (a) XRD pattern and the Rietveld refinement results of $PbCu_3Mn_4O_{12}$ at room temperature. The XRD pattern displays the observed (circles), calculated (red lines), and difference (olive line) profiles. Orange ticks indicate the Bragg reflections corresponding to this symmetry. The few unindexed diffraction peaks suggest the presence of small amounts of unidentified impurities. (b) Crystal structure of the A-site-ordered quadruple perovskite $PbCu_3Mn_4O_{12}$. This figure illustrates the arrangement of corner-sharing MnO_6 octahedra and square-planar CuO_4 units.

Table 1. Rietveld Refinement Results for $PbCu_3Mn_4O_{12}$ at Room Temperature[a]

parameter	value for $PbCu_3Mn_4O_{12}$
a (Å)	7.28930(1)
O_y	0.1829(3)
O_z	0.3053(3)
U_{iso} for Pb (100 × Å^2)	0.45(3)
U_{iso} for Cu (100 × Å^2)	0.47(3)
U_{iso} for Mn (100 × Å^2)	0.38(3)
U_{iso} for O (100 × Å^2)	0.49(9)
d_{Pb-O} (×12) (Å)	2.594(2)
d_{Cu-O} (×4) (Å)	1.947(2)
d_{Mn-O} (×6) (Å)	1.9294(7)
∠Mn−O−Mn (deg)	141.7(1)
∠Cu−O−Mn (deg)	109.01(6)
∠O−Cu−O (deg)	93.6(3)
∠O−Cu−O (deg)	86.4(1)
BVS (Cu)	1.93
BVS (Mn)	3.74
R_{wp} (%)	3.87
R_p (%)	2.63

[a]Space group: $Im\bar{3}$. Atomic sites: Pb 2a (0, 0, 0), Cu 6b (0, 0.5, 0.5), Mn 8c (0.25, 0.25, 0.25), and O 24g (0, y, z). The BVS values (V_i) were calculated via the formula $V_i = \sum_j S_{ij}$, where $S_{ij} = \exp[(r_0 - r_{ij})/0.37]$ using parameters $r_0(Cu^{2+}) = 1.679$ Å and $r_0(Mn^{4+}) = 1.753$ Å. 4-coordinated oxygen atoms were utilized for the A′-site Cu. 6-coordinated oxygen atoms were utilized for the B-site Mn.[26]

those of $CaCu_3Mn_4O_{12}$ (94.4°/85.6°), indicating smaller structural distortion of $PbCu_3Mn_4O_{12}$.[28] The bond-valence-sum (BVS) calculations indicate a valence state of +1.93 for the A′-site Cu and +3.74 for the B-site Mn, indicating a charge combination of $PbCu^{2+}{}_3Mn^{4+}{}_4O_{12}$, as further supported by XAS shown below. Regarding the A-site Pb, the Pb−O bond length is 2.59 Å, which is very similar to that observed in

https://doi.org/10.1021/acs.inorgchem.3c04493
Inorg. Chem. 2024, 63, 5924−5930

$Pb^{2+}VO_3$ (2.63 Å) but is significantly longer than that of $Pb^{4+}NiO_3$ (2.41 Å).[30,31] This suggests the presence of a Pb^{2+} charge state in $PbCu_3Mn_4O_{12}$. The tolerance factor (t) of $PbCu_3Mn_4O_{12}$ was determined based on the formula $t = (r_A + r_O)/\sqrt{2}(r_B + r_O)$, where r_A, r_O, and r_B represent the ion radii of A, O, and B, respectively. The calculated t = 0.81 indicates a stable perovskite structure for $PbCu_3Mn_4O_{12}$.

To further determine the valence states of the transition metals, XAS spectra were collected at the Cu and Mn $L_{2,3}$-edges. This technique is highly sensitive to the local electronic environment and valence states.[32,33] Figure 2a shows the XAS

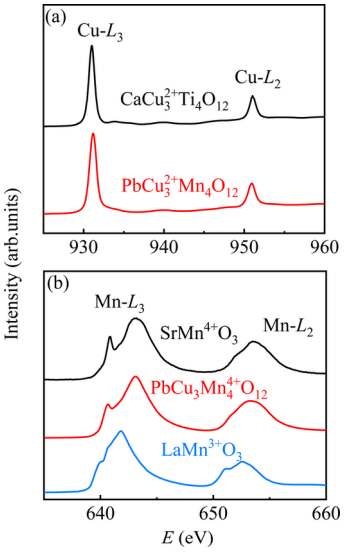

Figure 2. (a) XAS spectra of Cu $L_{2,3}$-edges for $PbCu_3Mn_4O_{12}$ along with $CaCu_3^{2+}Ti_4O_{12}$ as a Cu^{2+} reference. (b) XAS spectra of Mn $L_{2,3}$-edges for $PbCu_3Mn_4O_{12}$ along with $LaMn^{3+}O_3$ as a Mn^{3+} reference and $SrMn^{4+}O_3$ as a Mn^{4+} reference.

spectra at the Cu $L_{2,3}$-edges of $PbCu_3Mn_4O_{12}$ compared to $CaCu_3^{2+}Ti_4O_{12}$ as a Cu^{2+} reference with a similar square-planar CuO_4 coordination.[34−36] One can find that the energy positions of the single symmetry peak in $PbCu_3Mn_4O_{12}$ closely resemble those of $CaCu_3^{2+}Ti_4O_{12}$, indicating the presence of Cu^{2+} in $PbCu_3Mn_4O_{12}$. Figure 2b displays the XAS spectra at the Mn $L_{2,3}$-edges of $PbCu_3Mn_4O_{12}$, utilizing $LaMn^{3+}O_3$ as a Mn^{3+} reference and $SrMn^{4+}O_3$ as a Mn^{4+} reference with similar MnO_6 octahedral coordination.[37,38] Notably, the Mn $L_{2,3}$-edges spectrum of $PbCu_3Mn_4O_{12}$ exhibits a remarkable energy shift of approximately 1 eV to a higher energy compared to $LaMn^{3+}O_3$. However, it aligns closely with the energy position of $SrMn^{4+}O_3$, indicating the presence of the Mn^{4+} valence state in $PbCu_3Mn_4O_{12}$. Therefore, the charge combination of $PbCu_3Mn_4O_{12}$ is confirmed to be $Pb^{2+}Cu_3^{2+}Mn_4^{4+}O_{12}$.

Figure 3a illustrates the temperature-dependent ZFC and FC magnetic susceptibility curves for $PbCu_3Mn_4O_{12}$ measured under a field of 1000 Oe. It can be found that the magnetic susceptibility exhibits a sharp increase as the temperature decreases, reaching T_C of approximately 287 K, suggesting the occurrence of a ferromagnetic or ferrimagnetic phase transition. The T_C value is determined using the tangent method, as depicted in Figure 3a. Above T_C (320−380 K), the inverse susceptibility was well-fitted by the Curie−Weiss law using the function $\chi^{-1} = (T - \theta)/C$, where θ is the Weiss temperature and C is the Curie constant. The fitting results in θ = 284 K and C = 6.63 emu·K·mol^{-1}·Oe^{-1}. The positive value

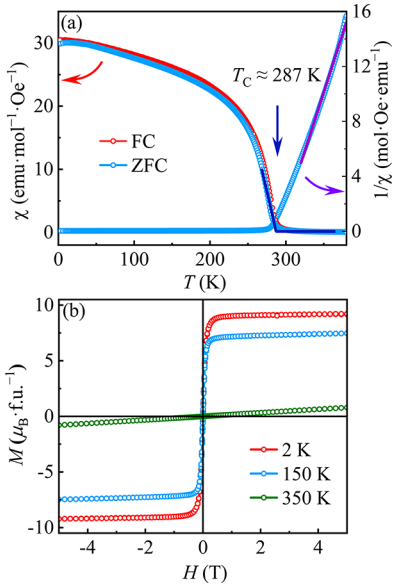

Figure 3. (a) Temperature-dependent magnetic susceptibility χ measured under the field of 1000 Oe using ZFC and FC modes, along with the inverse magnetic susceptibility, for $PbCu_3Mn_4O_{12}$. The purple line indicates the Curie−Weiss fitting between 320 and 380 K. A tangent method determines T_C to be 287 K. (b) Field-dependent magnetization for $PbCu_3Mn_4O_{12}$ collected at 2, 150, and 350 K.

of θ indicates a strong ferromagnetic interaction, and the absolute value of θ is very close to that of T_C. According to the fitted C, the effective magnetic moment is determined to be μ_{eff} = 7.28 μ_B·fu^{-1}, which is slightly smaller than the spin-only theoretical value μ_{cal} = 8.31 μ_B·fu^{-1} when considering the contributions of the Cu^{2+} ($3d^9$) and Mn^{4+} ($3d^3$) ions. Figure 3b displays the field-dependent magnetization measured at different temperatures. Above T_C, such as at 350 K, the magnetization curve exhibits linear behavior corresponding to the paramagnetic state. However, below T_C, for instance, at 150 and 2 K, typical magnetic hysteresis behaviors are observed, consistent with a ferromagnetic or ferrimagnetic state. The saturated moment obtained at 2 K and 5 T is 9.22 μ_B·fu^{-1}, which is much smaller than the calculated theoretical value of 15 μ_B·fu^{-1} for $Cu^{2+}(\uparrow)-Mn^{4+}(\uparrow)$ ferromagnetic coupling but very close to 9 μ_B·fu^{-1} for $Cu^{2+}(\uparrow)-Mn^{4+}(\downarrow)$ ferrimagnetic coupling. Therefore, the phase transition occurring at $T_C \approx$ 287 K is assigned to be ferrimagnetic.

Figure 4a presents the temperature dependence of the electrical resistivity measured under 0 and 8 T at 2−300 K. It can be observed that $PbCu_3Mn_4O_{12}$ exhibits semiconducting electrical transport behavior, characterized by the decrease of the resistivity with increasing temperature. Above 190 K, the temperature dependence of the resistivity can be well-fitted using the thermal activation model with the formula $\rho(T) = \rho(0)\exp[-(E_a/k_BT)]$, where $\rho(0)$ represents a preexponential factor, E_a is the activation energy, and k_B denotes Boltzmann's constant.[39] Fitting results are plotted in the inset of Figure 4a. Based on the fitted activation energy (E_a = 0.108 eV), the energy band gap (E_g) of $PbCu_3Mn_4O_{12}$ is estimated to be approximately 0.2 eV.[40,41] This value is relatively wider compared to the reported energy band-gap values of 0.12 eV for $CaCu_3Mn_4O_{12}$ and 0.13 eV for $MnCu_3Mn_4O_{12}$.[42] When an 8 T external magnetic field is applied, a significant decrease in the resistivity is observed, indicating the presence of a negative MR effect. The calculated MR values {=100% × [$\rho(H)$ −

https://doi.org/10.1021/acs.inorgchem.3c04493
Inorg. Chem. 2024, 63, 5924−5930

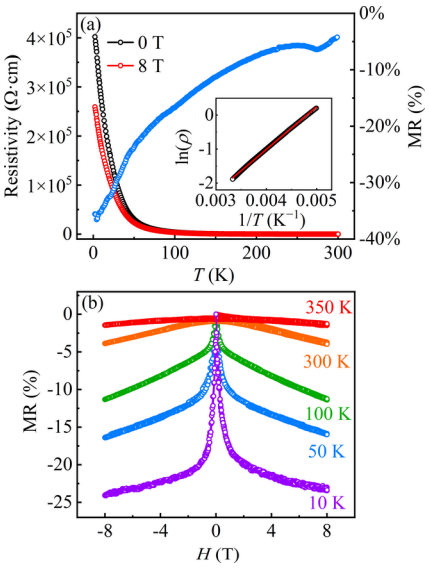

Figure 4. (a) Temperature-dependent resistivity for $PbCu_3Mn_4O_{12}$ below 300 K measured under 0 and 8 T. The MR between these two fields was also calculated and is displayed on the right side. The fitting result between 190 and 300 K based on the thermal activation model is displayed in the inset. (b) Field-dependent MR measured at fixed temperatures.

$\rho(0)]/\rho(0)\}$ between 0 and 8 T are consistently negative, and their absolute magnitude gradually increases with decreasing temperature, exhibiting an anomaly near T_C (as shown on the right side of Figure 4a). Additionally, $PbCu_3Mn_4O_{12}$ exhibits pronounced low-field MR effects. Figure 4b illustrates that, at 10 K and 1 T, the MR value is −19.76%, and it further decreases to −24.08% at 8 T, which is comparable to the observed MR of −22% at 2 K and 8 T in $MnCu_3Mn_4O_{12}$ but lower than the MR of −40.3% at 20 K and 5 T reported in $CaCu_3Mn_4O_{12}$.[14,22]

The heat capacity analysis provides further insight into the magnetic and electronic properties of $PbCu_3Mn_4O_{12}$. Figure 5

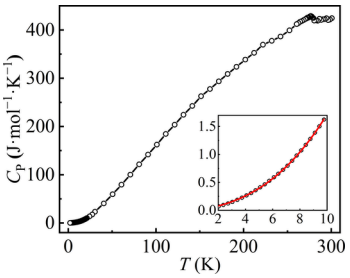

Figure 5. Temperature-dependent specific heat for $PbCu_3Mn_4O_{12}$ below room temperature. The inset shows the fitting results (red line) between 2 and 10 K using the formula $C_P = \alpha T^{3/2} + \beta T^3$.

displays the specific heat measurements for $PbCu_3Mn_4O_{12}$ in the temperature range of 2−300 K. First, a sharp λ-type anomaly is observed near T_C, confirming the previously mentioned long-range ferrimagnetic phase transition. Below 10 K, the heat capacity data can be well-fitted by the formula $C_P = \alpha T^{3/2} + \beta T^3$ (as shown in the inset of Figure 4). In this formula, the $T^{3/2}$ term represents the contribution of the ferromagnetic contribution, while the T^3 term comes from the antiferromagnetic and phonon excitation. The coefficients are fitted to be $\alpha = 2.51 \times 10^{-2}$ J·mol^{-1}·K$^{-5/2}$ and $\beta = 9.26 \times 10^{-4}$ J·mol^{-1}·K^{-4}. Furthermore, the absence of a T term in the specific heat fitting is also consistent with the semiconducting electric transport behavior. Similar fitting results are observed in $MnCu_3Mn_4O_{12}$.[22]

$PbCu_3Mn_4O_{12}$ shows a remarkable difference in the magnetic property compared to other members in the $ACu_3Mn_4O_{12}$ family with A = Mn, Cd, and Ca.[21,22,28] Specifically, there is a considerable reduction in T_C for $PbCu_3Mn_4O_{12}$ (Figure 6a). Due to the identical charge

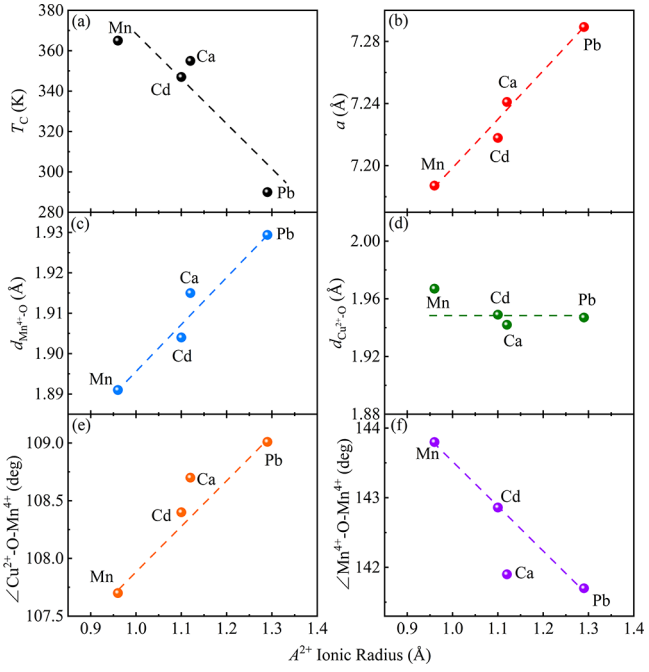

Figure 6. Evolution of (a) T_C, (b) unit-cell parameters a, (c) Mn^{4+}−O distance, (d) Cu^{2+}−O bond lengths, (e) Cu^{2+}−O−Mn^{4+} bond angles, and (f) Mn^{4+}−O−Mn^{4+} bond angles for $A^{2+}Cu_3Mn_4O_{12}$ with the A^{2+} ionic radius. Dashed lines are guides for eyes, and an 8-coordinated A^{2+} ionic radius was used for comparison.

configuration of $A^{2+}Cu_3^{2+}Mn_4^{4+}O_{12}$ as well as the ferrimagnetic spin alignment of $Cu^{2+}(\uparrow)$−$Mn^{4+}(\downarrow)$, the reduction of T_C is mainly attributed to the slightly different structural connection. Parts b and c of Figure 6 represent the evolution of the unit-cell parameter a and Mn^{4+}−O bond lengths of $A^{2+}Cu_3Mn_4O_{12}$ as a function of the A^{2+} ionic radius. As demonstrated in Figure 6b,c, the unit-cell parameter a and Mn^{4+}−O bond lengths increase with increasing A^{2+} ionic size, indicating a loose perovskite framework. This may reduce the 3d−2p orbital overlap and suppress the Cu^{2+}−O−Mn^{4+} superexchange interaction, leading to the decreasing T_C, while the Cu^{2+}−O bond lengths are virtually unchanged (Figure 6d), like the trend presented in $RECu_3Mn_4O_{12}$ (RE = rare-earth ions).[17] Moreover, the 90° superexchange pathway between the A′-site Cu^{2+} with a $3d^9(t_{2g}^6e_g^3)$ electronic configuration and B-site Mn^{4+} with a $3d^3(t_{2g}^3)$ configuration is predicted to be antiferromagnetic on the basis of the Goodenough−Kanamori−Anderson rules.[42−45] The deviation of Cu^{2+}−O−Mn^{4+} bond angles from 90° will further weaken the antiferromagnetic Cu^{2+}−O−Mn^{4+} superexchange interaction. As the A-site ionic size increases, the Cu^{2+}−O−Mn^{4+} bond angles also increase (Figure 6e), while the Mn^{4+}−O-Mn^{4+} bond angles decrease (Figure 6f). Because $PbCu_3Mn_4O_{12}$

https://doi.org/10.1021/acs.inorgchem.3c04493
Inorg. Chem. 2024, 63, 5924−5930

possesses the largest Cu^{2+}−O−Mn^{4+} bond angle in the family of $A^{2+}Cu_3Mn_4O_{12}$, this compound exhibits a relatively low T_C.

4. CONCLUSIONS

In conclusion, we successfully synthesized the near-room-temperature ferrimagnetic semiconductor $PbCu_3Mn_4O_{12}$ at 10 GPa and 1523 K for the first time. XRD indicates that $PbCu_3Mn_4O_{12}$ forms a A-site quadruple perovskite structure with the space group $Im\bar{3}$. According to the BVS calculations and XAS results, the charge combination was identified as $PbCu^{2+}{}_3Mn^{4+}{}_4O_{12}$. A ferrimagnetic phase transition was observed at $T_C \approx 287$ K due to the antiferromagnetic coupling between $Cu^{2+}(\uparrow)$ and $Mn^{4+}(\downarrow)$ ions. Moreover, $PbCu_3Mn_4O_{12}$ also exhibits semiconducting electric transport behavior with $E_g \approx 0.2$ eV and considerable low-field MR effects. Compared to other isostructural $ACu_3Mn_4O_{12}$ compounds with A = Mn, Cd, and Ca, there is a considerable reduction in T_C for $PbCu_3Mn_4O_{12}$ due to the elongation of unit-cell parameter a and Mn^{4+}−O bond lengths as well as a greater deviation of the Cu^{2+}−O−Mn^{4+} bond angle from 90°. The present work provides an intrinsic near-room-temperature ferrimagnetic semiconductor that holds promising potential for applications in next-generation spintronic devices.

■ ASSOCIATED CONTENT

Accession Codes

CCDC 2315609 contains the supplementary crystallographic data for this paper. These data can be obtained free of charge via www.ccdc.cam.ac.uk/data_request/cif, or by emailing data_request@ccdc.cam.ac.uk, or by contacting The Cambridge Crystallographic Data Centre, 12 Union Road, Cambridge CB2 1EZ, UK; fax: +44 1223 336033.

■ AUTHOR INFORMATION

Corresponding Author

Youwen Long − *Beijing National Laboratory for Condensed Matter Physics, Institute of Physics, Chinese Academy of Sciences, Beijing 100190, China; School of Physical Sciences, University of Chinese Academy of Sciences, Beijing 100049, China; Songshan Lake Materials Laboratory, Dongguan, Guangdong 523808, China;* orcid.org/0000-0002-8587-7818; Email: ywlong@iphy.ac.cn

Authors

Haoting Zhao − *Beijing National Laboratory for Condensed Matter Physics, Institute of Physics, Chinese Academy of Sciences, Beijing 100190, China; College of Materials Science and Opto-Electronic Technology, University of Chinese Academy of Sciences, Beijing 100049, China;* orcid.org/0009-0007-9656-5709

Dabiao Lu − *Beijing National Laboratory for Condensed Matter Physics, Institute of Physics, Chinese Academy of Sciences, Beijing 100190, China; School of Physical Sciences, University of Chinese Academy of Sciences, Beijing 100049, China;* orcid.org/0009-0006-5489-2835

Xiao Wang − *Beijing National Laboratory for Condensed Matter Physics, Institute of Physics, Chinese Academy of Sciences, Beijing 100190, China;* orcid.org/0000-0001-8139-4192

Xubin Ye − *Beijing National Laboratory for Condensed Matter Physics, Institute of Physics, Chinese Academy of Sciences, Beijing 100190, China;* orcid.org/0000-0002-5739-8318

Jie Zhang − *Beijing National Laboratory for Condensed Matter Physics, Institute of Physics, Chinese Academy of Sciences, Beijing 100190, China; School of Physical Sciences, University of Chinese Academy of Sciences, Beijing 100049, China;* orcid.org/0009-0006-9055-2969

Maocai Pi − *Beijing National Laboratory for Condensed Matter Physics, Institute of Physics, Chinese Academy of Sciences, Beijing 100190, China; School of Physical Sciences, University of Chinese Academy of Sciences, Beijing 100049, China*

Zhao Pan − *Beijing National Laboratory for Condensed Matter Physics, Institute of Physics, Chinese Academy of Sciences, Beijing 100190, China;* orcid.org/0000-0002-8693-2508

Yi-Ying Chin − *Department of Physics, National Chung Cheng University, Chiayi 621301, Taiwan;* orcid.org/0000-0003-2316-0747

Chien-Te Chen − *National Synchrotron Radiation Research Center (NSRRC), Hsinchu Science Park, Hsinchu 300092, Taiwan*

Zhiwei Hu − *Max Planck Institute for Chemical Physics of Solids, Dresden 01187, Germany;* orcid.org/0000-0003-0324-2227

Complete contact information is available at: https://pubs.acs.org/10.1021/acs.inorgchem.3c04493

Notes

The authors declare no competing financial interest.

■ ACKNOWLEDGMENTS

This work was supported by the National Key R&D Program of China (Grant 2021YFA1400300), the Beijing Natural Science Foundation (Grant Z200007), the National Natural Science Foundation of China (Grants 11934017, 12261131499, 11921004, 12304159, and 12304268), and the Chinese Academy of Sciences (Grant XDB33000000). We acknowledge support from the Max Planck POSTECH Hsinchu Center for Complex Phase Materials.

■ REFERENCES

(1) Zhou, L.; Dai, J.; Chai, Y.; Zhang, H.; Dong, S.; Cao, H.; Calder, S.; Yin, Y.; Wang, X.; Shen, X.; Liu, Z.; Saito, T.; Shimakawa, Y.; Hojo, H.; Ikuhara, Y.; Azuma, M.; Hu, Z.; Sun, Y.; Jin, C.; Long, Y. Realization of Large Electric Polarization and Strong Magnetoelectric Coupling in $BiMn_3Cr_4O_{12}$. *Adv. Mater.* **2017**, *29*, 1703435.

(2) Wang, X.; Chai, Y.; Zhou, L.; Cao, H.; Cruz, C. D.; Yang, J.; Dai, J.; Yin, Y.; Yuan, Z.; Zhang, S.; Yu, R.; Azuma, M.; Shimakawa, Y.; Zhang, H.; Dong, S.; Sun, Y.; Jin, C.; Long, Y. Observation of Magnetoelectric Multiferroicity in a Cubic Perovskite System: $LaMn_3Cr_4O_{12}$. *Phys. Rev. Lett.* **2015**, *115*, 087601.

(3) Johnson, R. D.; Chapon, L. C.; Khalyavin, D. D.; Manuel, P.; Radaelli, P. G.; Martin, C. Giant improper ferroelectricity in the ferroaxial magnet $CaMn_7O_{12}$. *Phys. Rev. Lett.* **2012**, *108*, 067201.

(4) Zhao, J.; Gao, J.; Li, W.; Qian, Y.; Shen, X.; Wang, X.; Shen, X.; Hu, Z.; Dong, C.; Huang, Q.; Cao, L.; Li, Z.; Zhang, J.; Ren, C.; Duan, L.; Liu, Q.; Yu, R.; Ren, Y.; Weng, S. C.; Lin, H. J.; Chen, C. T.; Tjeng, L. H.; Long, Y.; Deng, Z.; Zhu, J.; Wang, X.; Weng, H.; Yu, R.; Greenblatt, M.; Jin, C. A combinatory ferroelectric compound bridging simple ABO_3 and A-site-ordered quadruple perovskite. *Nat. Commun.* **2021**, *12*, 747.

(5) Yagi, S.; Yamada, I.; Tsukasaki, H.; Seno, A.; Murakami, M.; Fujii, H.; Chen, H.; Umezawa, N.; Abe, H.; Nishiyama, N.; Mori, S. Covalency-reinforced oxygen evolution reaction catalyst. *Nat. Commun.* **2015**, *6*, 8249.

https://doi.org/10.1021/acs.inorgchem.3c04493
Inorg. Chem. 2024, 63, 5924−5930

(6) Ye, X.; Song, S.; Li, L.; Chang, Y.-C.; Qin, S.; Liu, Z.; Huang, Y.-C.; Zhou, J.; Zhang, L.-j.; Dong, C.-L.; Pao, C.-W.; Lin, H.-J.; Chen, C.-T.; Hu, Z.; Wang, J.-Q.; Long, Y. A'-B Intersite Cooperation-Enhanced Water Splitting in Quadruple Perovskite Oxide $CaCu_3Ir_4O_{12}$. *Chem. Mater.* **2021**, *33*, 9295.
(7) Long, Y. W.; Hayashi, N.; Saito, T.; Azuma, M.; Muranaka, S.; Shimakawa, Y. Temperature-induced A-B intersite charge transfer in an A-site-ordered $LaCu_3Fe_4O_{12}$ perovskite. *Nature* **2009**, *458*, 60.
(8) Yamada, I.; Takata, K.; Hayashi, N.; Shinohara, S.; Azuma, M.; Mori, S.; Muranaka, S.; Shimakawa, Y.; Takano, M. A perovskite containing quadrivalent iron as a charge-disproportionated ferrimagnet. *Angew. Chem., Int. Ed.* **2008**, *47*, 7032.
(9) Yamada, I.; Etani, H.; Murakami, M.; Hayashi, N.; Kawakami, T.; Mizumaki, M.; Ueda, S.; Abe, H.; Liss, K. D.; Studer, A. J.; Ozaki, T.; Mori, S.; Takahashi, R.; Irifune, T. Charge-order melting in charge-disproportionated perovskite $CeCu_3Fe_4O_{12}$. *Inorg. Chem.* **2014**, *53*, 11794.
(10) Yamada, I.; Shiro, K.; Etani, H.; Marukawa, S.; Hayashi, N.; Mizumaki, M.; Kusano, Y.; Ueda, S.; Abe, H.; Irifune, T. Valence transitions in negative thermal expansion material $SrCu_3Fe_4O_{12}$. *Inorg. Chem.* **2014**, *53*, 10563.
(11) Kim, S. K.; Beach, G. S. D.; Lee, K.-J.; Ono, T.; Rasing, T.; Yang, H. Ferrimagnetic spintronics. *Nat. Mater.* **2022**, *21*, 24.
(12) Zhang, Y.; Feng, X.; Zheng, Z.; Zhang, Z.; Lin, K.; Sun, X.; Wang, G.; Wang, J.; Wei, J.; Vallobra, P.; He, Y.; Wang, Z.; Chen, L.; Zhang, K.; Xu, Y.; Zhao, W. Ferrimagnets for spintronic devices: From materials to applications. *Appl. Phys. Rev.* **2023**, *10*, 011301.
(13) Emori, S.; Li, P. Ferrimagnetic insulators for spintronics: Beyond garnets. *J. Appl. Phys.* **2021**, *129*, 020901.
(14) Zeng, Z.; Greenblatt, M.; Subramanian, M. A.; Croft, M. Large low-field magnetoresistance in perovskite-type $CaCu_3Mn_4O_{12}$ without double exchange. *Phys. Rev. Lett.* **1999**, *82*, 3164.
(15) Sánchez-Benítez, J.; Prieto, C.; de Andrés, A.; Alonso, J. A.; Martínez-Lope, M. J.; Casais, M. T. Evidence of two differentMnstates in $CaCu_3Mn_4O_{12}$ derivatives with colossal magnetoresistance. *Phys. Rev. B* **2004**, *70*, 024419.
(16) Zhang, Q.; Bréard, Y.; Guillou, F.; Hardy, V. Investigation of the magnetocaloric effect in double distorted perovskites $(Cu_{3-x}Mn_x)Mn_4O_{12}$ $(1 \leq x \leq 2)$: From standard ferrimagnetism to glassy ferrimagnetism. *Phys. Rev. B* **2011**, *84*, 224430.
(17) Sanchez-Benitez, J.; Alonso, J. A.; Martinez-Lope, M. J.; de Andres, A.; Fernandez-Diaz, M. T. Enhancement of the Curie temperature along the perovskite series $RCu_3Mn_4O_{12}$ driven by chemical pressure of R^{3+} cations (R = rare earths). *Inorg. Chem.* **2010**, *49*, 5679.
(18) Alonso, J. A.; Sánchez-Benıtez, J.; De Andrés, A.; Martınez-Lope, M. J.; Casais, M. T.; Martınez, J. L. Enhanced magnetoresistance in the complex perovskite $LaCu_3Mn_4O_{12}$. *Appl. Phys. Lett.* **2003**, *83*, 2623.
(19) Saito, T.; Chen, W.-t.; Mizumaki, M.; Attfield, J. P.; Shimakawa, Y. Magnetic coupling between A′ and B sites in theA-site-ordered perovskite $BiCu_3Mn_4O_{12}$. *Phys. Rev. B* **2010**, *82*, 024426.
(20) Takata, K.; Yamada, I.; Azuma, M.; Takano, M.; Shimakawa, Y. Magnetoresistance and electronic structure of the half-metallic ferrimagnet $BiCu_3Mn_4O_{12}$. *Phys. Rev. B* **2007**, *76*, 024429.
(21) Sánchez-Benítez, J.; Kayser, P.; Morales-García, Á.; Martínez-Lope, M. J.; Mompeán, F. J.; Xu, J.; Jin, Z.; Alonso, J. A. Preparation, Crystal Structure, and Magnetotransport Properties of the New $CdCu_3Mn_4O_{12}$ Perovskite: A Comparison with Density Functional Theory Calculations. *J. Phys. Chem. C* **2014**, *118*, 9652.
(22) Guo, J.; Wang, S.; Li, W.; Lu, D.; Ye, X.; Liu, Z.; Qin, S.; Wang, X.; Hu, Z.; Lin, H.-J.; Chen, C.-T.; Wan, J.; Zhang, Q.; Long, Y. A-site Mn^{2+} tuned magnetism and electrical transport properties in the transition-metal-only perovskite oxide $MnCu_3Mn_4O_{12}$. *Phys. Rev. B* **2022**, *105*, 054409.
(23) Shpanchenko, R. V.; Chernaya, V. V.; Tsirlin, A. A.; Chizhov, P. S.; Sklovsky, D. E.; Antipov, E. V.; Khlybov, E. P.; Pomjakushin, V.; Balagurov, A. M.; Medvedeva, J. E.; Kaul, E. E.; Geibel, C. Synthesis, structure, and properties of new perovskite $PbVO_3$. *Chem. Mater.* **2004**, *16*, 3267.
(24) Shirane, G.; Pepinsky, R.; Frazer, B. C. X-Ray and Neutron Diffraction Study of Ferroelectric $PbTiO_3$. *Phys. Rev.* **1955**, *97*, 1179.
(25) Larson, A. C.; Von Dreele, R. B. *General Structure Analysis System (GSAS)*; Los Alamos National Laboratory: Los Alamos, NM, 1994; Report No. LAUR 86-748.
(26) Brown, I. D.; Altermatt, D. Bond-valence parameters obtained from a systematic analysis of the inorganic crystal structure database. *Acta Crystallogr., Sect. B: Struct. Sci.* **1985**, *41*, 244.
(27) Vasil'ev, A. N.; Volkova, O. S. New functional materials $AC_3B_4O_{12}$ (Review). *Low Temp. Phys.* **2007**, *33*, 895.
(28) Chenavas, J.; Joubert, J. C.; Marezio, M.; Bochu, B. The synthesis and crystal structure of $CaCu_3Mn4O_{12}$: A new ferromagnetic-perovskite-like compound. *J. Solid State Chem.* **1975**, *14*, 25.
(29) Shannon, R. D. Revised effective ionic radii and systematic studies of interatomic distances in halides and chalcogenides. *Acta Cryst. A* **1976**, *32*, 751.
(30) Belik, A. A.; Azuma, M.; Saito, T.; Shimakawa, Y.; Takano, M. Crystallographic Features and Tetragonal Phase Stability of $PbVO_3$, a New Member of $PbTiO_3$ Family. *Chem. Mater.* **2005**, *17*, 269.
(31) Inaguma, Y.; Tanaka, K.; Tsuchiya, T.; Mori, D.; Katsumata, T.; Ohba, T.; Hiraki, K.; Takahashi, T.; Saitoh, H. Synthesis, structural transformation, thermal stability, valence state, and magnetic and electronic properties of $PbNiO_3$ with perovskite- and $LiNbO_3$-type structures. *J. Am. Chem. Soc.* **2011**, *133*, 16920.
(32) Nemrava, S.; Vinnik, D. A.; Hu, Z.; Valldor, M.; Kuo, C.-Y.; Zherebtsov, D. A.; Gudkova, S. A.; Chen, C.-T.; Tjeng, L. H.; Niewa, R. Three Oxidation States of Manganese in the Barium Hexaferrite $BaFe_{12-x}Mn_xO_{19}$. *Inorg. Chem.* **2017**, *56*, 3861.
(33) Tjeng, L.; Chen, C.; Cheong, S.-W. Comparative soft-x-ray resonant-photoemission study on $Bi_2Sr_2CaCu_2O_8$, CuO, and Cu_2O. *Phys. Rev. B* **1992**, *45*, 8205.
(34) McGuinness, C.; Downes, J. E.; Sheridan, P.; Glans, P. A.; Smith, K. E.; Si, W.; Johnson, P. D. X-ray spectroscopic study of the electronic structure of the high-dielectric-constant material $CaCu_3Ti_4O_{12}$. *Phys. Rev. B* **2005**, *71*, 195111.
(35) Liu, Z.; Sun, Q.; Ye, X.; Wang, X.; Zhou, L.; Shen, X.; Chen, K.; Nataf, L.; Baudelet, F.; Agrestini, S.; Chen, C.-T.; Lin, H.-J.; Vasili, H. B.; Valvidares, M.; Hu, Z.; Yang, Y.-f.; Long, Y. Quadruple perovskite oxide $LaCu_3Co_2Re_2O_{12}$: A ferrimagnetic half metal with nearly 100% B-site degree of order. *Appl. Phys. Lett.* **2020**, *117*, 152402.
(36) Ye, X.; Liu, Z.; Wang, W.; Hu, Z.; Lin, H. J.; Weng, S. C.; Chen, C. T.; Yu, R.; Tjeng, L. H.; Long, Y. High-pressure synthesis and spin glass behavior of a Mn/Ir disordered quadruple perovskite $CaCu_3Mn_2Ir_2O_{12}$. *J. Phys.: Condens. Matter* **2020**, *32*, 075701.
(37) Burnus, T.; Hu, Z.; Hsieh, H. H.; Joly, V. L. J.; Joy, P. A.; Haverkort, M. W.; Wu, H.; Tanaka, A.; Lin, H. J.; Chen, C. T.; Tjeng, L. H. Local electronic structure and magnetic properties of $LaMn_{0.5}Co_{0.5}O_3$ studied by x-ray absorption and magnetic circular dichroism spectroscopy. *Phys. Rev. B* **2008**, *77*, 125124.
(38) Sahu, R. K.; Hu, Z.; Rao, M. L.; Manoharan, S. S.; Schmidt, T.; Richter, B.; Knupfer, M.; Golden, M.; Fink, J.; Schneider, C. M. X-ray absorption spectra at the Ru and Mn $L_{2,3}$ edges and long-range ferromagnetism in $SrRu_{1-x}Mn_xO_3$ solid solutions $(0 \leq x \leq 0.5)$. *Phys. Rev. B* **2002**, *66*, 144415.
(39) Perlstein, J. H.; Sienko, M. J. Single-Crystal Studies of Electrical Conductivity, Seebeck Effect, and Hall Voltage in Sodium Vanadium Bronze and a Crystal-Field Model of Electron Transport. *J. Chem. Phys.* **1968**, *48*, 174.
(40) Huang, Y.; He, Y.; Skinner, B.; Shklovskii, B. I. Conductivity of two-dimensional narrow gap semiconductors subjected to strong Coulomb disorder. *Phys. Rev. B* **2022**, *105*, 054206.
(41) Skinner, B.; Chen, T.; Shklovskii, B. I. Why is the bulk resistivity of topological insulators so small? *Phys. Rev. Lett.* **2012**, *109*, 176801.
(42) Weht, R.; Pickett, W. E. Magnetoelectronic properties of a ferrimagnetic semiconductor: The hybrid cupromanganite $CaCu_3Mn_4O_{12}$. *Phys. Rev. B* **2001**, *65*, 014415.

https://doi.org/10.1021/acs.inorgchem.3c04493
Inorg. Chem. 2024, 63, 5924−5930

(43) Goodenough, J. B. Theory of the Role of Covalence in the Perovskite-Type Manganites[La, M(II)]MnO_3. *Phys. Rev.* **1955**, *100*, 564.
(44) Kanamori, J. Superexchange interaction and symmetry properties of electron orbitals. *J. Phys. Chem. Solids* **1959**, *10*, 87.
(45) Anderson, P. W. Antiferromagnetism. Theory of Superexchange Interaction. *Phys. Rev.* **1950**, *79*, 350.

https://doi.org/10.1021/acs.inorgchem.3c04493
Inorg. Chem. 2024, 63, 5924−5930